THERMALLY CHARGEABLE SUPERCAPACITOR WITH CHARGING AND DISCHARGING CYCLES FOR WEARABLE AND IOT ELECTRONICS

A Thesis

by

AQEEL MOHAMMED ABDUL MAGEETH

Submitted to the Office of Graduate and Professional Studies of
Texas A&M University
in partial fulfillment of the requirements for the degree of

MASTER OF SCIENCE

Chair of Committee,	Choongho Yu
Committee Members,	M. Cynthia Hipwell
	Micah Green
Head of Department,	Andreas A. Polycarpou

August 2019

Major Subject: Mechanical Engineering

ABSTRACT

Thermally chargeable supercapacitors are good candidates for energy harvesting and storage in wearable and internet-of-things (IoT) electronic devices. We report a Thermally chargeable supercapacitor (TCSC) which has good areal capacitance of 14.58 mF/cm^2 and charge storage capability in conjunction with a spiral bimetal coil and heat source to create an in-situ thermal cycling setup modeling real world application. The thermally chargeable supercapacitor (TCSC) has graphene oxide intercalated with sulfate ions (SGO) acting as electrolyte/separator and reduced sulfate graphene oxide (RSGO) electrodes fabricated by laser irradiation on a film of SGO over PET substrate using a 3D printer with laser diode assembly. The fabricated supercapacitor employs the soret effect as the transport mechanism, which results in high thermoelectric voltage. The TCSC showed improved capacitance and higher current output when electrode thickness and electrolyte concentration increased. Humid environments resulted in improved capacitance of the TCSC. The in situ thermal cycling setup was constructed by bending the TCSC with the help of aluminum foil as substrate. One end of the supercapacitor specimen placed over the bimetal coil with the attached end acting as the hot side and the end far away acting as the cold side. Thermal charging occurs when heat source is on causing the bimetal coil to detach from the surface and maintain the temperature gradient across the TCSC which leads to voltage generation. When heat source is off bimetal coil comes in contact with the heat source and temperature gradient drops close to zero. The TCSC produces a differential voltage of 10 mV for a temperature difference of 6K generated by programming the heat source close to human skin temperature of 34^0C. The in-

situ thermal cycling setup which is reported here gives us clarity on how the TCSC performs under human skin temperature conditions.

ACKNOWLEDGEMENTS

I would like to thank my committee chair Dr. Choongho Yu and my committee members Dr. M. Cynthia Hipwell and Dr. Micah Green for their constant support and guidance throughout the course of my research.

I would also like to thank my lab mates at Nano Energy Lab and the departmental staff for giving a great experience at Texas A&M University.

CONTRIBUTORS AND FUNDING SOURCES

Contributors

This work was supervised by a thesis committee consisting of Professor Choongho Yu and Professor M. Cynthia Hipwell of the Department of Mechanical Engineering and Professor Micah Green of the Department of Chemical Engineering. All other work for the thesis was completed by the student independently.

Funding Sources

There are no outside contributions to acknowledge related to the research and compilation of this document.

NOMENCLATURE

GO	Graphene Oxide
RSGO	Reduced Sulfate Graphene Oxide
SGO	Sulfate ion intercalated graphene oxide
H_2SO_4	Sulphuric Acid
TEG	Thermoelectric Generator
TCSC	Thermally chargeable supercapacitor
CV	Cyclic voltammetry

TABLE OF CONTENTS

Page

LIST OF FIGURES

Page

LIST OF TABLES

1. INTRODUCTION

Energy harvesting from human body and waste heat generating devices are of keen interest to the scientific community as they provide sustainable and clean energy[1, 2]. The major challenge is that waste heat is classified as low-quality energy. Thermoelectric generators(TEG) which work on seebeck effect[3-5] and made of inorganic materials are popular choice to achieve conversion of waste heat to useful energy, but the efficiency of these devices is low. Traditional thermoelectric materials have thermopower in the range of 10-100 μV/k[6, 7] and large number of generator modules are required to generate voltage and current for practical applications. In addition to it they are not suitable for wearable applications due to lack of flexibility. Thermally chargeable supercapacitors[8, 9] which utilize temperature gradient are ideal for energy harvesting and for wearable applications as they do not require an external wired power source and facilitate quick charging and discharging[10-15]. They are very flexible and do not exhibit loss in capacitance on bending. In this work, we seek to explore the best value which can be derived from this kind of supercapacitors .Graphene based supercapacitor are more suitable for this application because of high theoretical surface area, good electrical and thermal properties and flexibility of graphene[16-19]. In this work, a graphene oxide based Thermally chargeable supercapacitor(TCSC) is made using scalable laser[19-22] irradiation on SGO film on PET substrate enabled by a 3D printer with laser diode assembly as reported[9]. This TCSC has reduced sulfate graphene oxide (RSGO) as electrodes with SGO as the separator/electrolyte. The intercalation of sulfate ions into GO to form SGO results in high ionic conductivity hence providing a sound alternative to liquid electrolytes that are known to inhibit the operating voltage and give rise to leakage problems .The TCSC works on Soret effect, which is the diffusion of ions under temperature gradient[23-26] and charge is

stored like a pseudo capacitor resulting in large thermoelectric voltages compared to conventional inorganic thermoelectric devices. The goal is to achieve higher charge storage and current for practical application and hence larger and thicker modules are prepared compared to previous work. In principle, increase in electrode thickness increases the area of charge storage and hence increases the capacitance. It has already been reported that thermopower and electrical conductivity increases with relative humidity[9]. This finding provided the basis of studying the capacitance and current variation as a function of relative humidity. In this work emphasis is laid on the idea of making the TCSC cycle with temperature change by constructing an in-situ thermal cycling setup consisting of heat source and TCSC in conjunction with thin sensitive spiral bimetal coil which moves in response to temperature change. This behavior of bimetal coil can be used to create charging and discharging cycles for TCSC. Most of the research reported on supercapacitors have limited only to study of performance without an eye for making them commercially attractive[21, 27]. Thermal cycling can be extended to any type of supercapacitor devices which can work on temperature gradient thus having a very good potential impact. Many applications involving TEG have been reported like health monitoring using wireless communication protocol[28]. The power requirement for these applications is in the order of 50-100 μW. It is already reported that this graphene oxide based TCSC is capable of powering electrochromic device which has a voltage requirement of 2V[9]. In this work we scale up the supply current of TCSC by having larger and thicker TCSC modules and observe how it fares in temperature conditions close to human skin temperature. The energy storage of TCSC under these conditions are calculated to have an understanding of whether these devices can be practically rolled out to wearable and IOT electronics technology in terms of energy output generated.

2. RESEARCH OBJECTIVE

The purpose of this research work is to make a thermally chargeable supercapacitor which can harvest energy from waste heat and one which has great flexibility, compactness, performance and durability. The TCSC modules made in this work are larger and thicker to enhance the final current output. The focus lies on creating charging and discharging cycles which are temperature dependent and observing the voltage output response. This project explores temperature based thermal cycling for wearable devices. An experimental setup consisting of heat source, TCSC and spiral bimetal coil is used to demonstrate the phenomena of thermal cycling. The temperature-based movement of the TCSC attached with a bimetal coil will be tracked using an IR camera to capture the temperature gradient which can be used to calculate the energy storage. The deflection of the bimetal coil will be calculated. Finally, a detailed analysis and calculation of energy stored and efficiency of TCSC under conditions modeling human skin temperature will be carried out thus demonstrating its commercial viability and possibility of incorporation into wearable device technology.

3. MATERIALS AND METHODS

3.1 Preparation of TCSC

60-mg GO (Carbon solutions, Inc.) is dispersed in 30-mL deionized (DI) water to prepare a GO solution by sonication with a probe sonicator (100 W, XL2000, Misonix Micron) for 2h. SGO solutions is prepared by mixing the as-dispersed GO solution and 2M H_2SO_4 (1.65g), followed by 30-minute sonication. The solution is divided into two centrifuge tubes, then the SGO solution must be centrifuged at 8500 rpm for 15 min. The supernatant formed is removed and then the SGO is dispersed into DI water to make a solution with a concentration of 8 mg SGO/mL H_2O, then probe sonication is done for 2 hours. The resulting solution is drop casted on 2-inch x 2-inch PET film (5.33g solution)[9]. The sample is then dried in room temperature for 24 hours. For drawing RSGO electrodes, a 3D model as shown in Figure 1b is created in Solid works and file saved in stl format. The stl file is opened in Cura 3D printing software and rotated at 90^0 to initial orientation. The coordinates are set to (X, Y) = (-28, -20). The file is then saved in the SD card as "gcode" format. The SD card is inserted into 3D printer. The file is selected, and printing started. The Anet A8 3D printer with printer head replaced by sample holder in conjunction with a Thor Labs blue diode laser as shown in Figure 1a is used to draw the RSGO electrodes. The width and length of the TCSC sample used for all the tests is 1 inch and the thickness is 40 μm. The TCSC consists of 50 RSGO/SGO pairs meaning 50 capacitors in series. The schematic of TCSC is shown in Figure 1c. Figure 1d shows optical microscope image of TCSC taken using a 5X objective lens. The width of RSGO electrodes is almost half that of the SGO layer width.

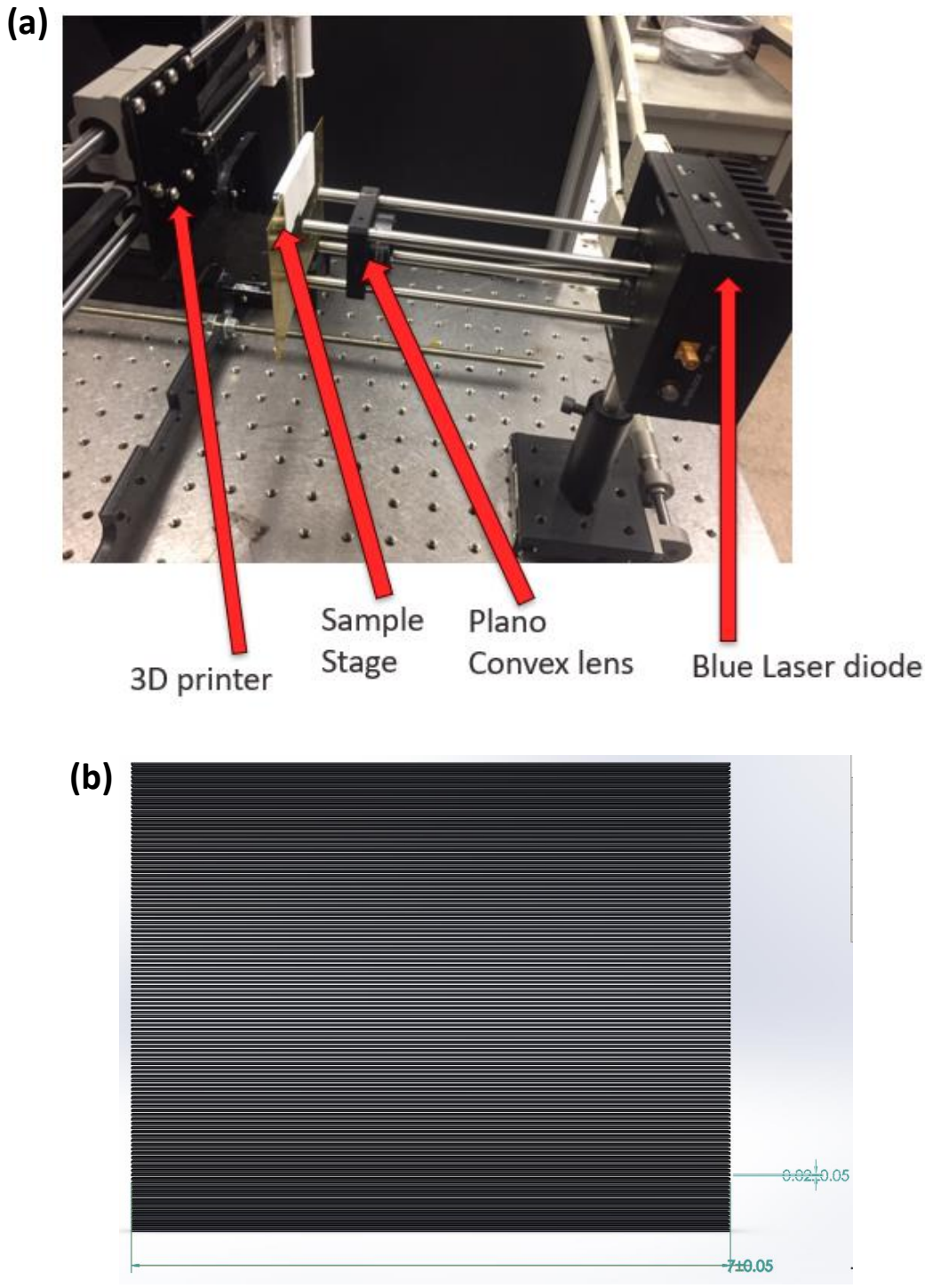

Figure 1. Fabrication of TCSC (a) 3D printer with laser diode assembly used for fabricating the TCSC. (b) 3D model in Solid works for drawing the electrodes. (c) Schematic of TCSC. (d) Optical microscope bright field image of TCSC using a 5X objective lens.

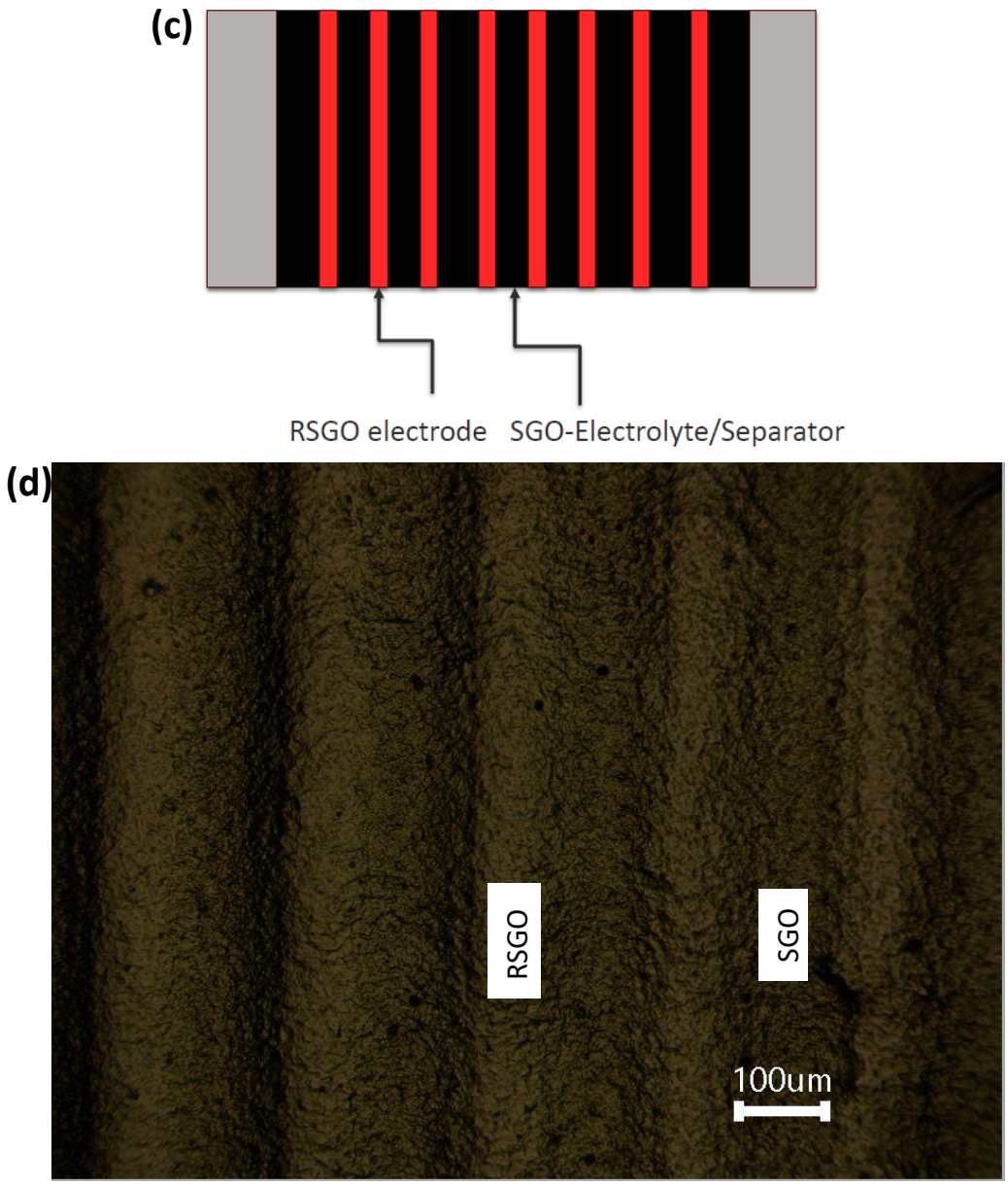

Figure 1. Continued.

3.2 Cyclic voltammetry and thermoelectric setup measurements

The cyclic voltammetry (CV) measurements for the TCSC was done in a CHI604D electrochemical station using 3-electrode system. The ends of the TCSC sample was painted using electron microscopy sciences Graphite conductive adhesive. One end was connected to the reference and counter electrode and the other end connected to working electrode for measurement. The TCSC was housed in humidity chamber with connecting alligator clips to the electrochemical workstation for CV measurements at different RH levels. For thermal charging and discharge response measurements a thermoelectric setup as shown in Figure 6a consisting of two Peltier devices grounded on an aluminum metal sink was used. Silver paint was applied to both ends of TCSC and the TCSC was placed with ends on both the Peltier devices. Keithley 2400 source meter was used to supply current for creation of temperature difference across the sample. T- type Thermocouples placed on the ends of TCSC in conjunction with a Lab view measurement program was used to record the temperature and voltage-time response. The galvanostatic charge discharge test and the capacitance retention of TCSC was done using a LAND battery tester. The ends of the TCSC was painted using graphite conductive adhesive with an aluminum foil placed on top for smooth connection to the electrode system.

3.3 In-situ thermal cycling setup

The In-situ thermal cycling setup as shown in Figure 7a consists of a wood sink over which a polyimide film heater (1-inch x 1 inch) with power rating of 5W/inch^2 is attached. A brass sheet of 250-micron thickness is placed over the heater such that heater is sandwiched between the wood sink and the brass sheet. Keithley 2400 source meter was used to power the heater. The heat flux

from the brass sheet is calculated by estimating temperature of the brass sheet using IR camera at steady state. The TCSC is placed over the brass sheet with one edge of the specimen over a spiral bimetal coil which is used to provide cyclic movement on temperature change. The TCSC is bent by gluing an aluminum foil beneath the PET substrate in order to produce a gradual temperature gradient across the length of the TCSC during thermal charging. T-type thermocouples attached at the ends of the TCSC in conjunction with a lab view measurement program was used to estimate the voltage difference across the TCSC. When the heat source is on, the coil moves up creating a temperature gradient in the TCSC and when the heat source is off the coil comes in contact with the sheet and the TCSC is in discharge state as the temperature difference across TCSC drops to zero. Human skin temperature conditions were obtained by programming the power supply Keithley 2400 to the desired supply current range and letting the heat source maintain the skin temperature of 34^0C.

4. RESULTS AND DISCUSSION

4.1 Electrochemical performance measurement of TCSC under different conditions

The TCSC sample was subjected to cyclic voltammetry (CV) measurements. Two TCSC samples with different quantity of SGO solution were made to study the effect of SGO film thickness on capacitance, one with 2.66 g of SGO solution drop casted in PET film and another with 5.33g (double the amount). The drop casting resulted in samples of 20µm and 40µm thickness respectively. The CV measurements were taken for both the samples at a relative humidity of 38% for scan rates of 10 mV/s, 20 mV/s, 50 mV/s and 100 mV/s as shown in Figure 2a and Figure 2b. The current window was found to be higher in Figure 2a than in Figure 2b for the same scanning potential range indicating the TCSC has better current characteristics when the SGO film layer was thicker. The area under the CV curve was found to be higher for the 40 µm thick sample for all the scan rates which tells capacitance is higher for 40µm sample. This is because higher the electrode thickness higher the area of charge storage for the in-plane capacitor resulting in higher capacitance. The capacitance is plotted vs scan rate for both the samples with varying SGO thickness in Figure 2c.

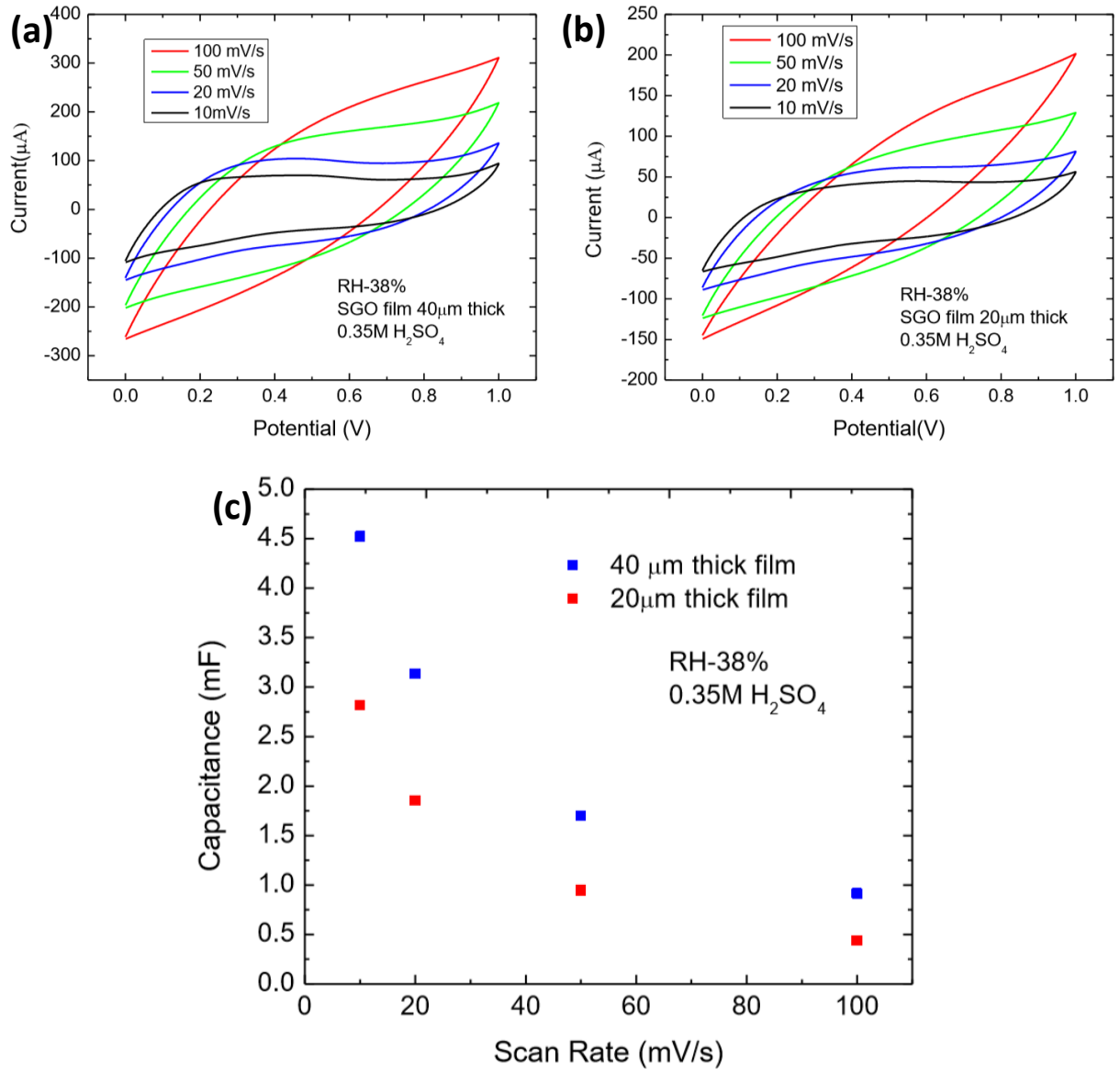

Figure 2. Effect of SGO film thickness on capacitance of TCSC. (a) CV curve of TCSC with SGO film 40 μm thick. (b) CV curve of TCSC with SGO film 20μm thick. (c) Capacitance comparison of SGO film of different thickness. The concentration of H_2SO_4 in the SGO solution was 0.35M and the RH level of the environment was 38%.

For studying the effect of concentration of H_2SO_4, two SGO solutions of different SGO concentrations were prepared, one with 0.35M(1.1 g of H_2SO_4) added in GO solution and another with 0.55M (1.65 g of H_2SO_4) in GO solution. The CV curves of TCSC samples with different SGO concentration is shown in Figure 3a and 3b. The current window is slightly higher for 0.55M H_2SO_4 sample. The higher current associated with the CV curve of 0.55M sample is because of higher proton concentration and electrical conductivity. The capacitance comparison as shown in Figure 3c did not yield a consistent trend. At scan rates of 10 mV/s and 20 mV/s the sample of higher concentration (0.55M) yielded higher capacitance but sample of lower concentration (0.35M) gave a higher capacitance at higher scan rate of 50 mV/s and 100 mV/s. This discrepancy is because there is higher rate of electrochemical degradation at higher scan rates for 0.55M sample because of higher pseudocapacitive component in the sample contributed by increased concentration of sulfate ions. It is clearly evident that the sample with SGO layer 40 μm thick (higher current and higher capacitance) and 0.55M concentration of H_2SO_4 (higher current) performed better hence for further tests the sample of 40μm thick with 0.55M SGO solution was used.

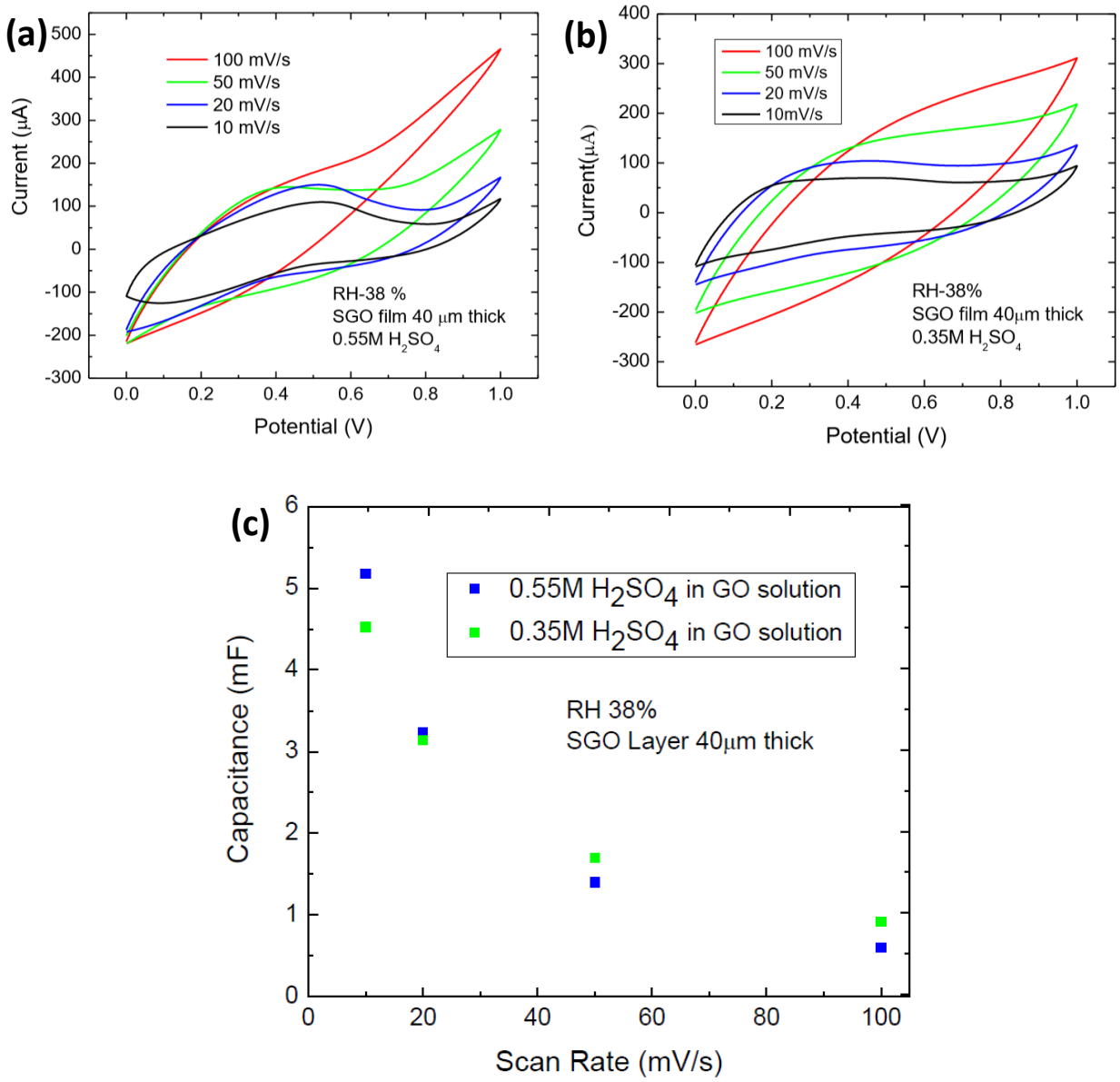

Figure 3. Effect of electrolyte concentration on the capacitance. (a) CV curve of TCSC made with SGO solution containing 0.55M H_2SO_4. (b) CV curve of TCSC made with SGO solution containing 0.35M H_2SO_4. (c) Capacitance comparison of TCSC with different concentrations of SGO solution. The SGO film was 40 μm thick and relative humidity of the environment was 38%.

The CV curves of the TCSC at different humidity levels for a scan rate of 10 mV/s are shown in Figure 4a. It can be clearly seen that the CV curve displayed flatter ellipsoids with rise in humidity levels. The current window of the CV curve also increased with higher RH for the same scanning potential range. The water uptake (% mass increase) variation with RH% is shown in Figure 4b which indicates the TCSC sample has high affinity to water. This is because the TCSC sample contains GO which is hydrophilic and H_2SO_4 which is also strongly hygroscopic in nature. The effect of capacitance with variation in relative humidity level is shown in Figure 4c. The capacitance doubled from 5.18mF at 38 % RH level to 10.39 mF at 82% RH level. The capacitance increase with RH can be attributed to more proton dissociation in the electrolyte and opening up of more conductive pathways leading to transfer of greater number of protons to the cold side on application of temperature gradient. This leads to increase in polarization across the electrodes contributing to a higher dielectric effect.

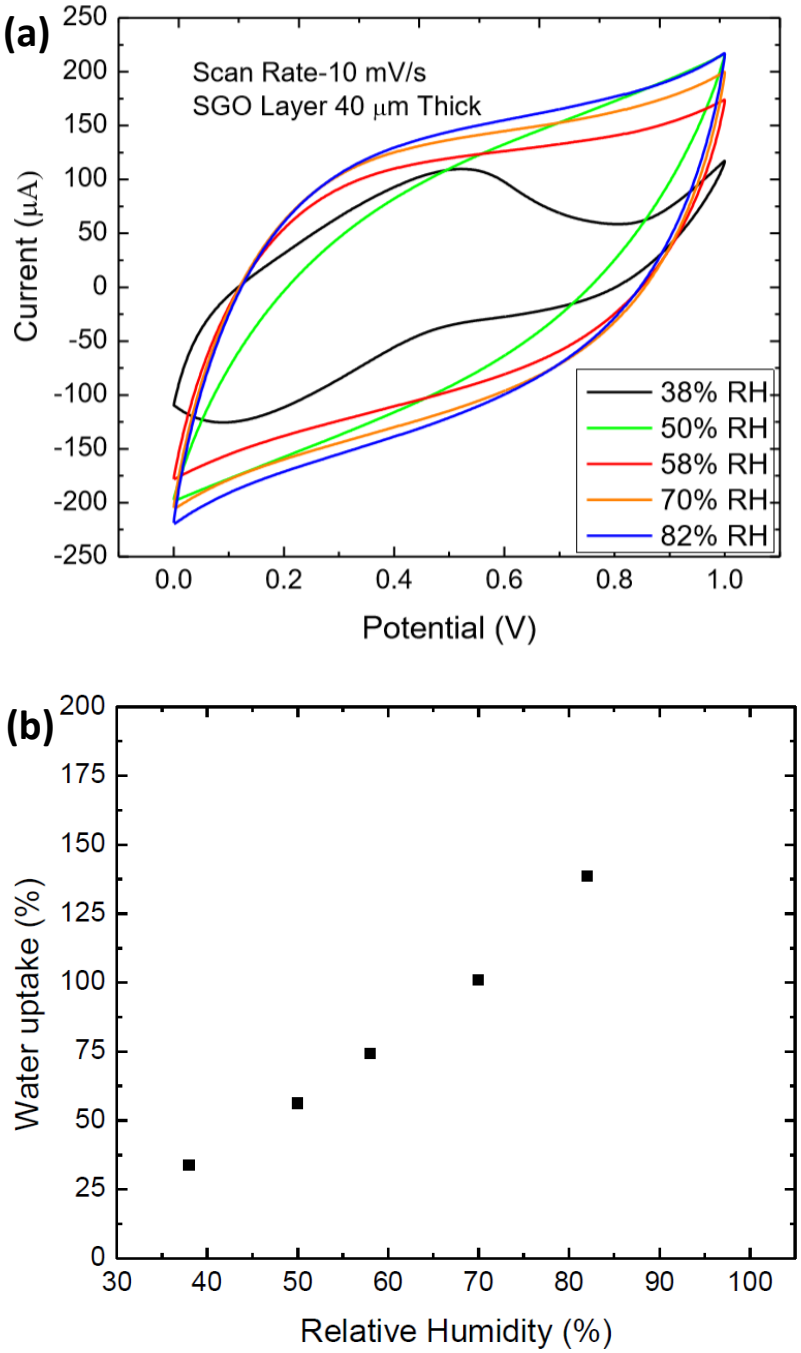

Figure 4. Effect of humidity on charge storage. (a) CV curves of TCSC at 10 mV/s scan rate at different relative humidity environment. (b) Variation of water uptake of TCSC with relative humidity. (c) Capacitance of TCSC under different relative humidity. The TCSC had 0.55M SGO solution and the SGO film was 40 μm thick.

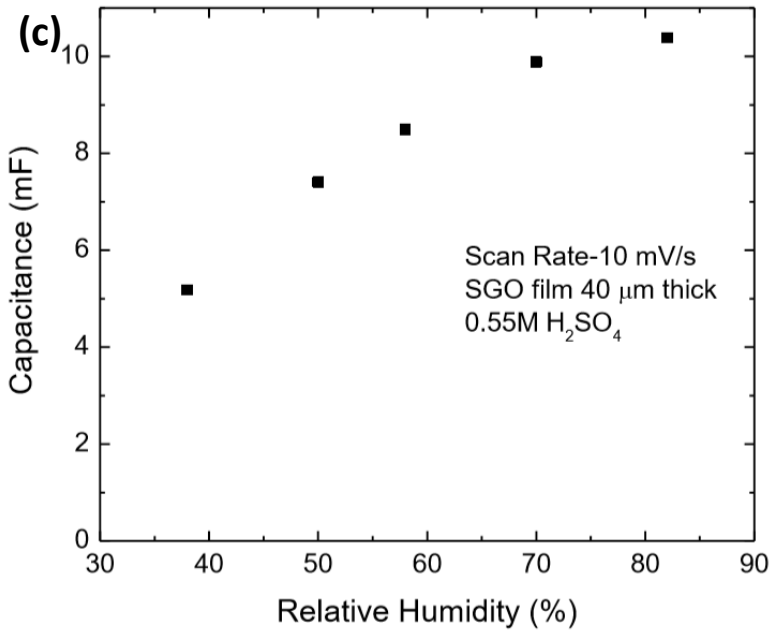

Figure 4. Continued.

The areal capacitance of TCSC reported here at 50% RH was 14.58 mF/cm^2 which is highest among other graphene[19] and graphene oxide-based supercapacitors[27, 29]. In this work we have higher overall charge storage and higher current (at least 5 times) than reported in [9] by having increased SGO film thickness and higher electrolyte concentration. The areal capacitance of this in plane TCSC is lower than other out of plane configuration thermally chargeable supercapacitors[8].This is because of higher pseudocapacitive mode of charge storage in [8]. The out of plane supercapacitors however are not that flexible and also fabrication is not scalable hence giving this in plane TCSC an upper hand in terms of ease of fabrication, design and incorporation into wearable device technology.

4.2 Galvanostatic charge discharge behavior of TCSC and capacitance retention

The Galvanostatic charge discharge curves of the TCSC are shown in Figure 5a. The test was done at four different current densities of 1 mA/cm^2, 2 mA/cm^2,5 mA/cm^2,10 mA/cm^2. The increase in current density decreased the charging and discharging time which was the desired trend. The TCSC showed moderate coulombic efficiency at all the current densities tested. The capacitance retention test was done for 2000 cycles at two different current densities 10 mA/cm^2 and 20 mA/cm^2. The results are shown in Figure 5b. The capacitance retention drop was around 10% for current density of 10 mA/cm^2 and 25% for a current density of 20 mA/cm^2. The capacitance drop in the TCSC for 2000 cycles is found to be nearly same as out of plane TCSC reported in [8] with higher current density of 10 mA/cm^2 used which indicates better retention compared to the out of plane TCSC. Increase in current density leads to decrease in capacitance retention as the TCSC is subjected to more cycles of operation. The current densities are significantly lower compared to those applied in the battery tester when TCSC is thermally charged hence the TCSC can show better capacitance retention with number of operating cycles during thermal charging and discharge operation.

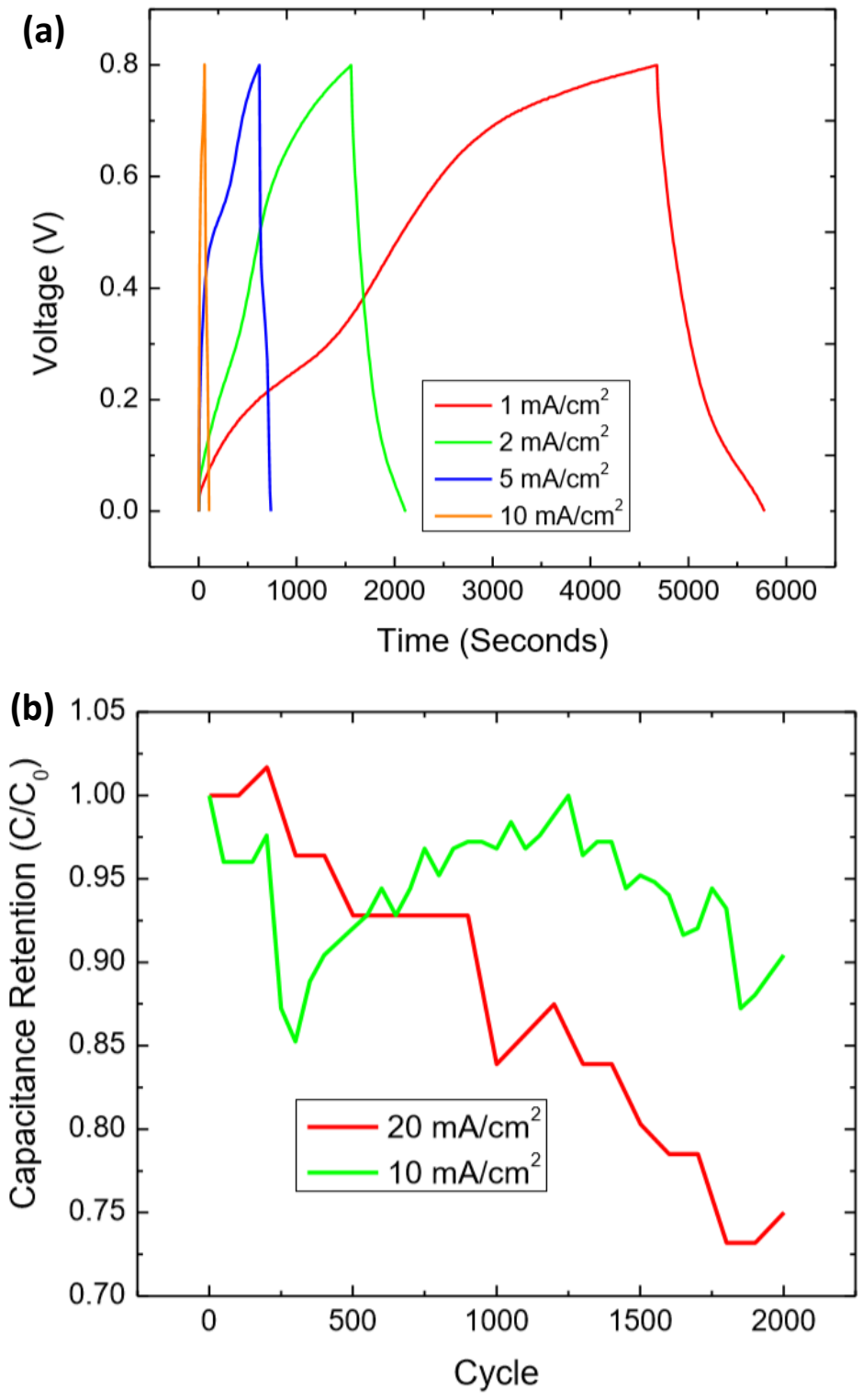

Figure 5. Electrical charge-discharge behavior of TCSC. (a) Galvanostatic charge-discharge behavior. (b) Capacitance Retention.

4.3 Thermal charging and discharging behavior of TCSC

The thermal charging and discharging behavior testing of TCSC was carried out in a thermoelectric measurement setup. The TCSC is placed over two peltier devices one for the hot side and another one for the cold side as shown in Figure 6a. Both the peltier devices are grounded to an aluminum heat sink. The power supply to the peltier devices was programmed to give different temperature gradients across the TCSC. The voltage generation from TCSC recorded under different temperature gradients is shown in Figure 6b. The environment was at 50% RH during testing. The charge stored per unit area reached a maximum of 894 $\mu C/cm^2$ for a temperature gradient of 14 K. This is at least five times greater than the value reported in the previous work[9]. The relationship between the voltage generated and temperature difference was linear with R^2 value of 0.976 which is close to 1. The device seebeck was calculated by estimating the slope of the graph in Figure 6b which was 4.53 mV/k. This tells us that the TCSC is capable of generating 4.53 mV per degree of temperature gradient. The voltage time response of the TCSC was recorded as shown in Figure 6c by programming the peltier device in order to generate a temperature difference around 4.5K. When the power supply was turned on to generate temperature difference across TCSC thermal charging occurred and the voltage attained a peak of 28.1 mV in 370 seconds (thermal charging time). After the voltage attained a peak and the peltier devices still in ON condition, a 2kΩ load resistor was connected across the TCSC. This resulted in thermal discharge and the voltage attained a value of zero as the resistor was connected. After this stage the peltier devices were switched off making the temperature difference across TCSC converge to zero but the voltage showed an increase in the negative direction and stabilized at same peak value after long time. This voltage is due to the electron flow to the cold side of the TCSC when the load resistor was

connected. The electrons get accumulated in the cold side and when the temperature difference became zero eventually which lead to protons in the cold side go back to random positions. The voltage generated due to the accumulated electrons is the one which is extractable from the TCSC for practical purposes.

(a)

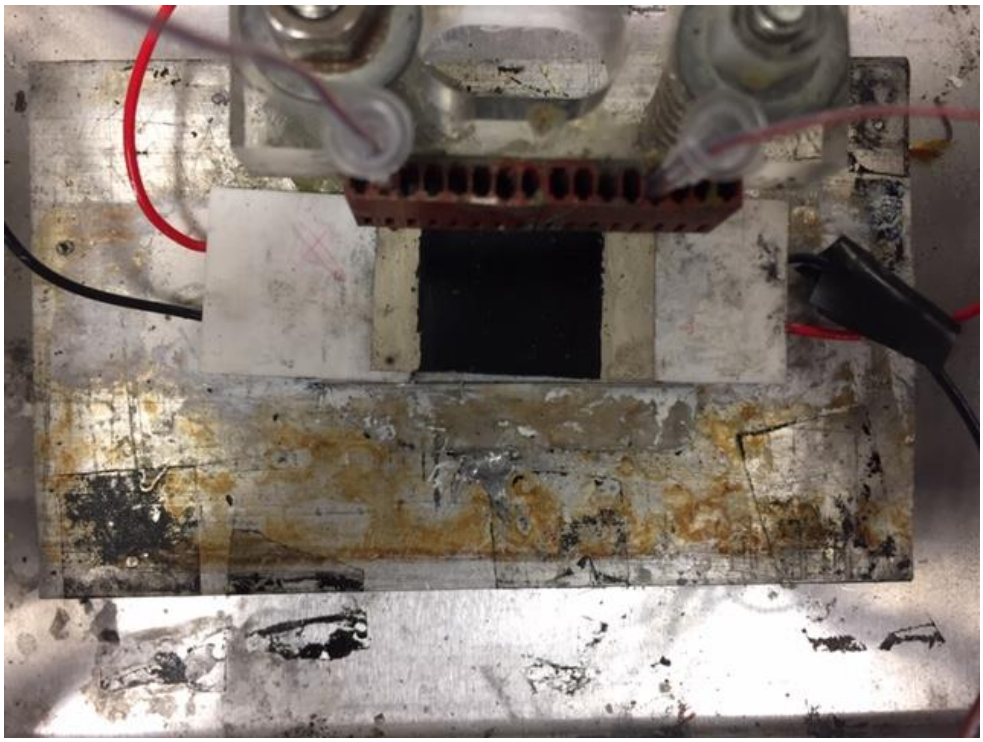

Figure 6. Thermoelectric setup voltage measurement. (a) Thermoelectric measurement setup image. (b) Voltage generated by TCSC under different temperature gradients. (c) Voltage response of TCSC and temperature difference across TCSC recorded with time.

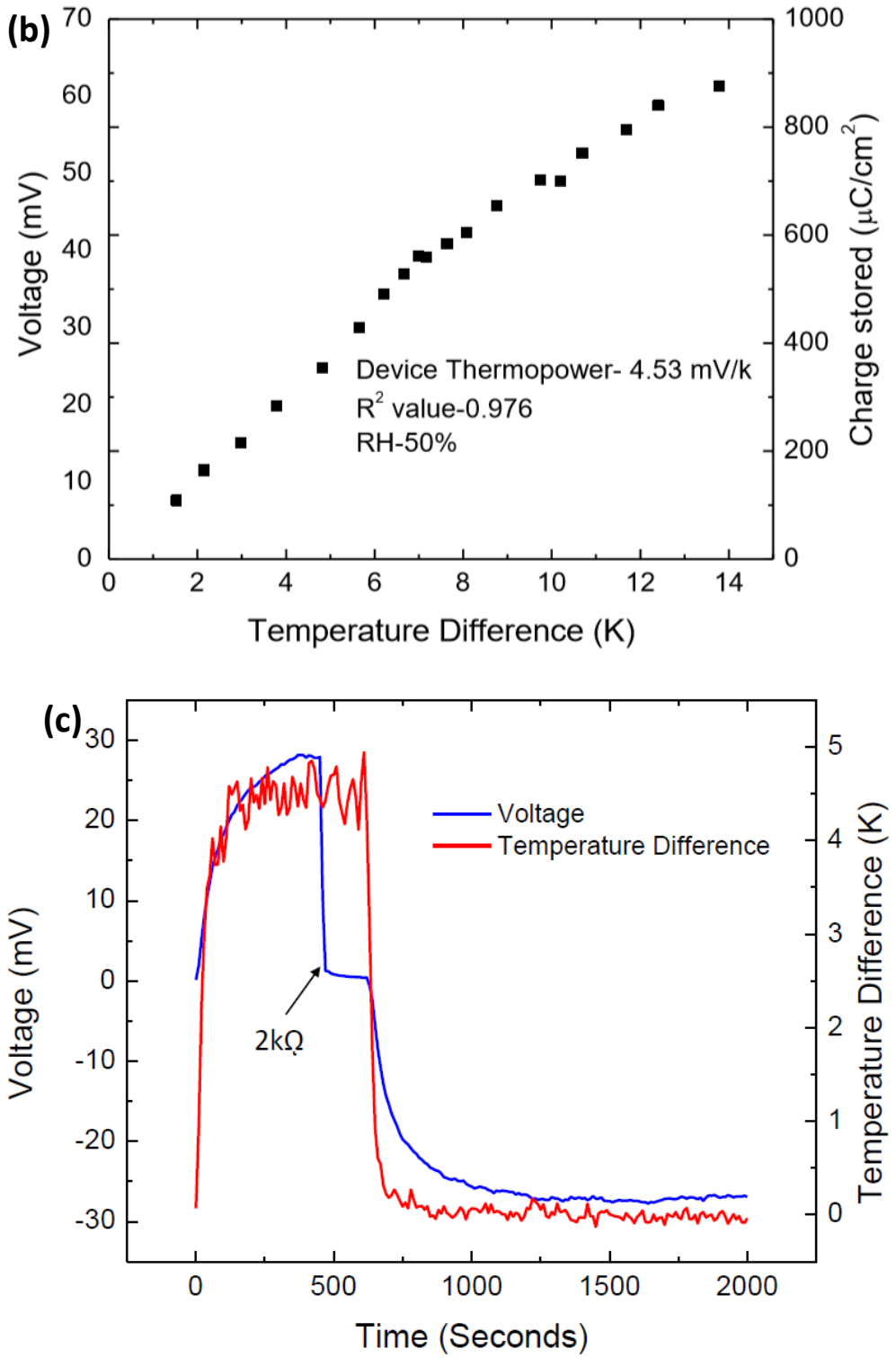

Figure 6. Continued.

4.4 In-situ performance testing of TCSC

The in-situ thermal cycling setup was used to estimate the voltage generation of TCSC under more realistic conditions of device operation. The in-situ thermal cycling setup consists of only one heat source without a heat sink in contrast to the thermoelectric measurement setup which has a heat source and heat sink. The in-situ setup is different from the thermoelectric measurement setup in the aspect that the TCSC is subjected to heat source at one end which is the hot side and the other end is left free and protected from the heat source by using rubber packing as radiation shield. This end acts as cold side. The hot side of the TCSC is attached to spiral bimetal coil as shown in Figure 7a. Initially at the beginning of in-situ performance testing the bimetal is in the position touching the heat source as shown in Figure 8a. The temperature difference across the TCSC before the heater is ON is zero. The corresponding point of this position in the voltage-time response plot as shown in the Figure 7b and Figure 7c is point 1 and the IR camera image at the initial position is shown in Figure 7d numbered as 1. The visible image is shown in Figure 7e. When the heat source is ON the bimetal slowly lifts up as shown in Figure 8b. Thermal charging occurs as the bimetal lifts up slowly and the voltage reaches a peak at point 2 in the voltage-time response plot as shown in Figure 7b and 7c. The IR camera image at point 2 is shown in Figure 7d image 2 which gives the temperature gradient of 4K across TCSC and the corresponding heat source temperature at the peak point 2. The heat source is turned off when the voltage is at peak and voltage drops to point 3. The IR image of point 3 is shown in image number 3 of Figure 7d. The bimetal comes back to original position contacting the heat source as shown in Figure 8a. The temperature difference is close to zero but however we have a residual voltage at this point. This is because the in-situ setup does not have a proper heat sink which is grounded like the thermoelectric measurement setup

where both the cold side and hot side of the TCSC where grounded to aluminum heat sink. The role of the bimetal coil is to maintain the temperature gradient produced during thermal charging. The cycle of testing is repeated to record the voltage-time response under higher temperature gradients of 6K and 8K. The corresponding peak points and IR images are indicated in Figure 7b,7c and 7d respectively. When the heat source is programmed to human skin temperature of 34^0C, the temperature gradient across the TCSC was 6K and the differential voltage generated was 10.02 mV. The point corresponding to this condition of TCSC is shown in Figure 7d image number 4. The energy stored in the TCSC was calculated using the relation $W=1/2*C*V^2$, where C is 7.41 mF and differential voltage V is 10.02 mV and W was $3.71*10^{-7}$ J. The value reported here is comparable to other thermoelectric capacitors which have been demonstrated for energy harvesting from body heat and known to produce a voltage of 81 mV and energy stored of 2.8 μJ[30] around the same temperature difference but at higher RH% than reported here. The voltage for a given temperature difference estimated from the in-situ setup is lower than that estimated from thermoelectric measurement setup because the IR camera was used for temperature difference estimation in the in-situ setup which is less accurate compared to the T-type thermocouple used in the thermoelectric measurement setup.

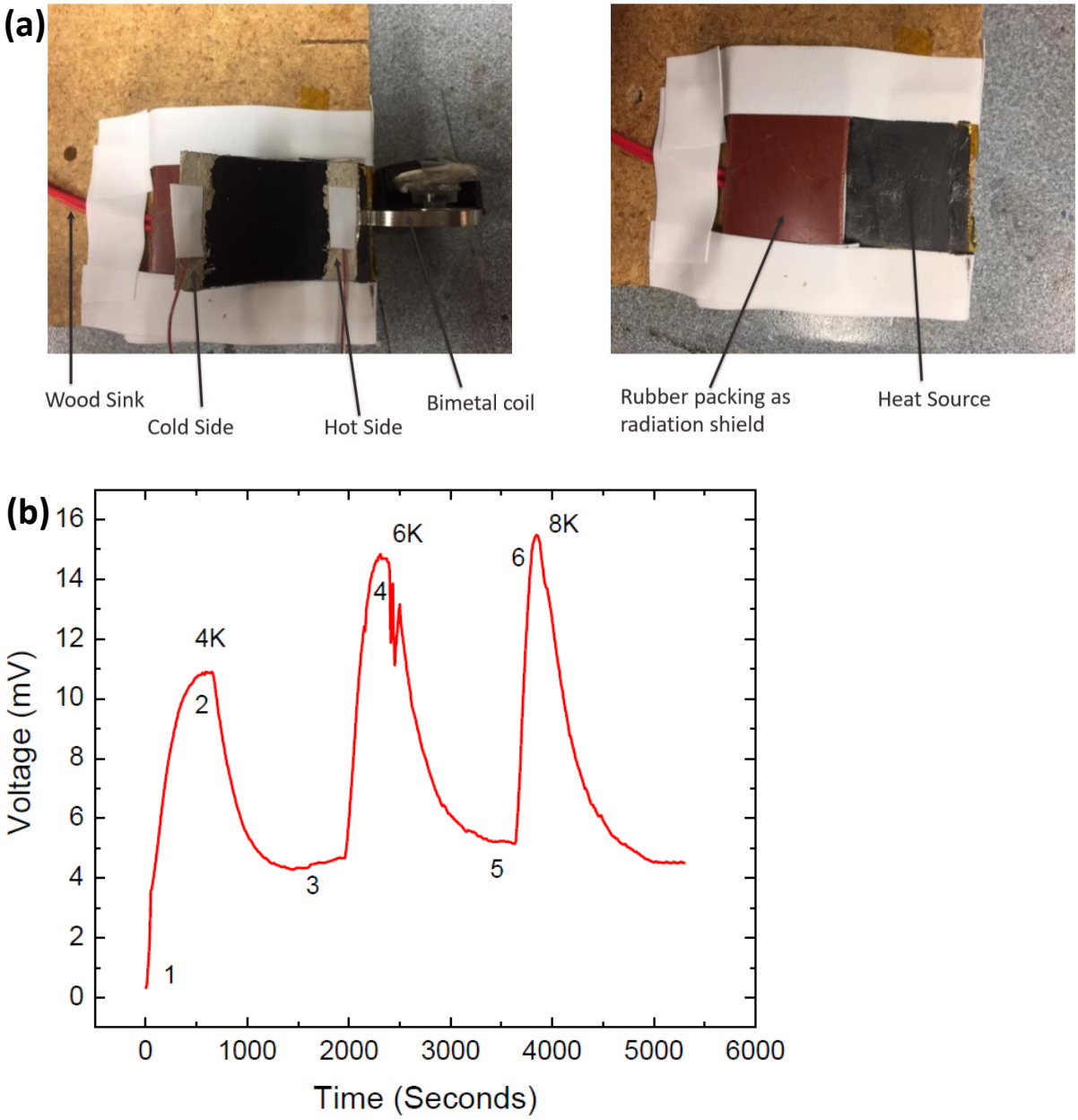

Figure 7. In-situ performance testing of TCSC. (a) Image of in-situ thermal cycling setup. (b) Voltage response with time for different temperature gradients in the in-situ thermal cycling setup. (c) Differential voltage versus time for different temperature gradients in the in-situ thermal cycling setup. (d) IR images of the in-situ thermal cycling setup recording different temperature gradients across TCSC. The images shown are corresponding from point 1-6. (e) Visible counterpart image of point 1.

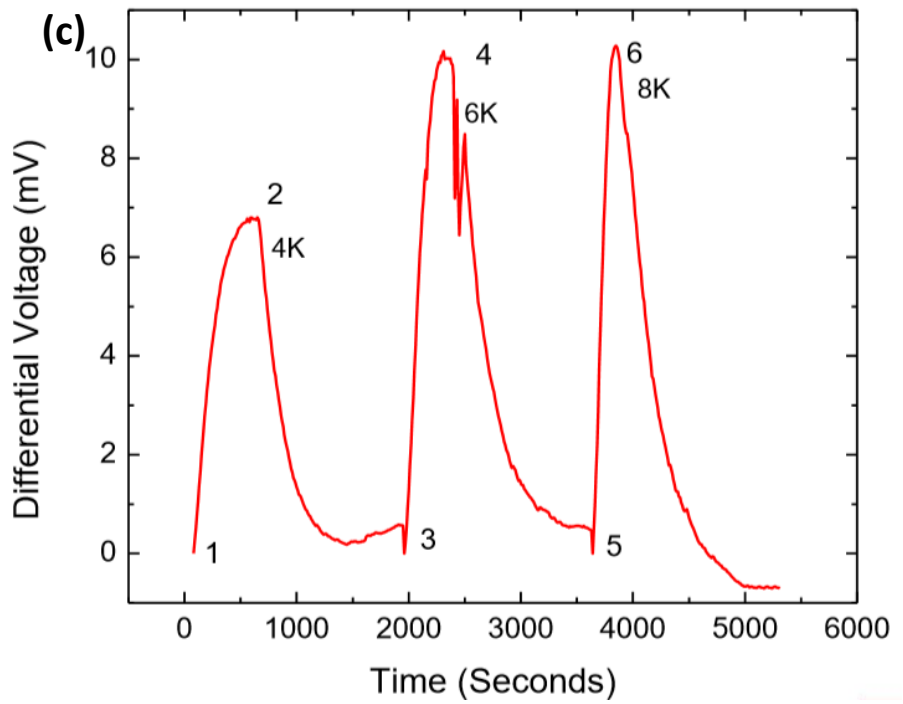

Figure 7. Continued.

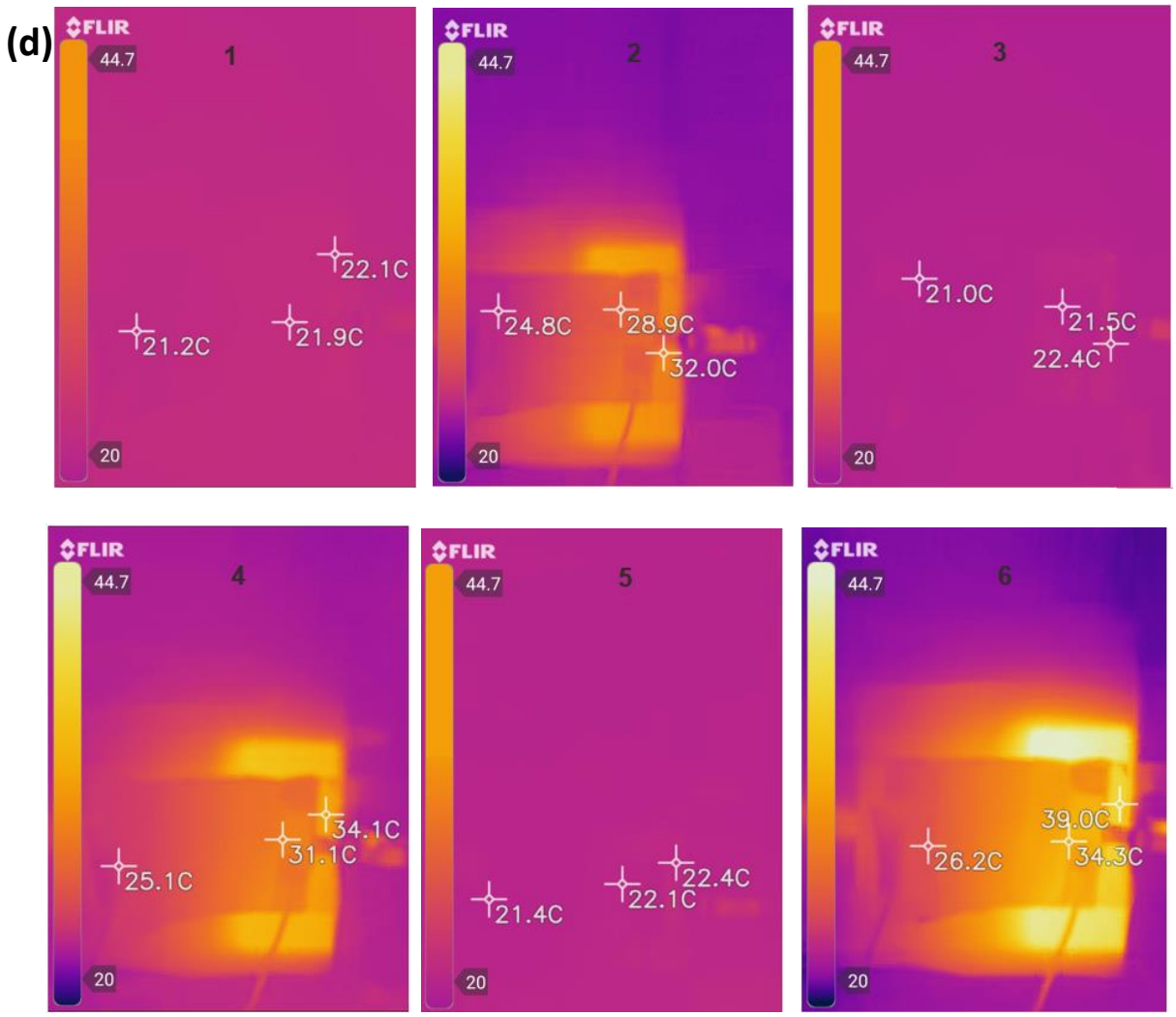

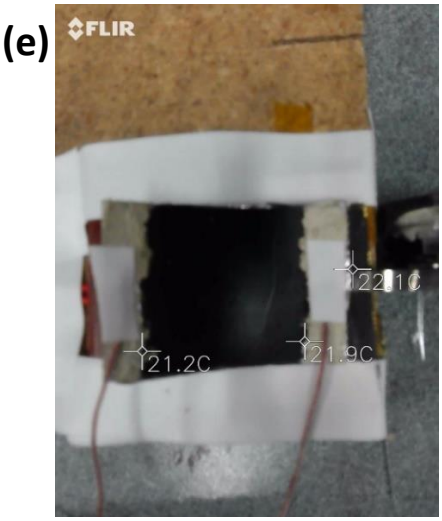

Figure 7. Continued.

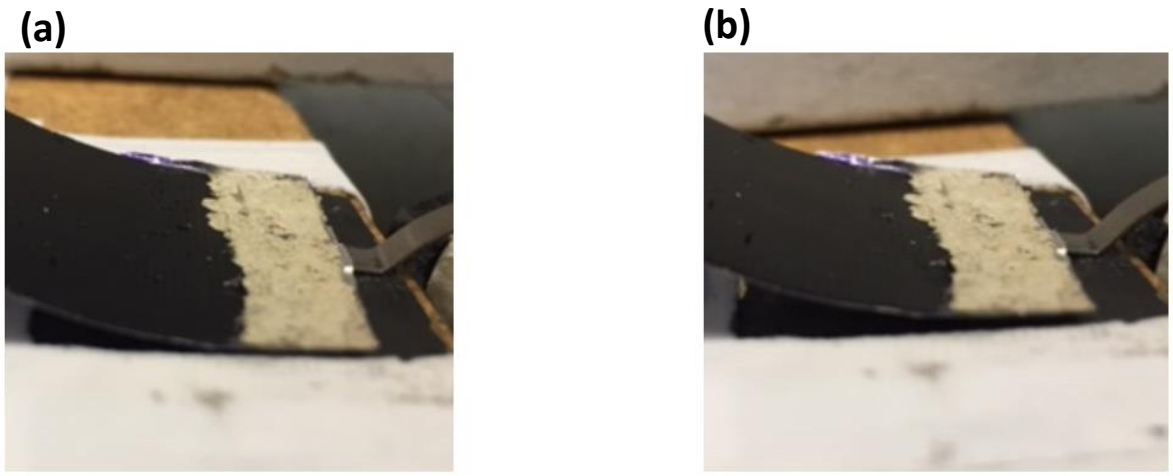

Figure 8. In-situ bimetal-TCSC movement. (a) Heat source in OFF condition. (b) Heat source in ON condition.

4.5 Energy storage and Efficiency of In-situ system

The energy storage analysis of TCSC was done by assuming only radiation energy input from heat source to TCSC hot side and rest of the TCSC is shielded from radiation by rubber packing acting as radiation shield as shown in Figure 7a. The heat source is painted black so that we can assume emissivity equal to 1 for calculation purposes. The heat flux by conduction from heat source to bimetal is considered negligible as the contact area of bimetal with heat source is very less and it becomes zero in a few seconds as bimetal goes off contact with increase in temperature of heat source. The temperature difference of 6K was generated when the heat source temperature was 34^0C as shown in Figure 7d image 4. The heat source was programmed to the human skin temperature of 34^0C to observe the performance of TCSC under skin temperature conditions. For the temperature difference of 6K the maximum output voltage generated by TCSC is around 10.02 mV. The capacitance of the 1-inch x 1-inch TCSC was found to be 7.41 mF from the CV curve results. The energy stored was calculated by $W= (1/2) *C*V^2$, where C is the capacitance and V is the differential voltage of the TCSC at the peak point. For a temperature difference of 6K, the energy stored was 3.71×10^{-7} J. The heat flux radiated out of the heat source to the bimetal was calculated with the help of data from Figure 7d image 4 and using the equation $Q_s=(J_1-J_2)$, where Q_s is heat flux radiated out of the heat source to the TCSC hot side,J_1-Radiosity of heat source, J_2-Radiosity of TCSC. The radiation heat input to TCSC is calculated by $q=Q_s*a*t$, where a-Area of TCSC hot side, t-time taken to reach the peak voltage which is estimated from the in-situ voltage response plot Figure 7c.The deflection of the bimetal was calculated by $S= (A*L^2*dt)/T$, where S is deflection of bimetal, A is thermal coefficient of expansion of bimetal (steel and brass), L is length of the bimetal exposed to heated surface, dt- Temperature difference, T is thickness of the

bimetal. The deflection of bimetal from heat source when the heat source is switched on is used to estimate the view factor F_{12}. The view factor calculated was close to 1 because of very small deflection of bimetal. The efficiency of the system is calculated by taking the ratio of energy stored to the heat energy input. The calculated values are shown in Table 1.

Table 1. Energy storage analysis of TCSC for Human skin temperature conditions

Heat Flux from heat source to TCSC (W/m^2)	Q_s	2.92
Area of TCSC hot side (cm^2)	a	1.612
Deflection of bimetal (mm)	S	0.19
Capacitance (mF)	C	7.41
Areal Capacitance (mF/cm^2)	C_a	14.58
Voltage (mV)	V	10.02
Energy stored in TCSC (J)	W	3.71×10^{-7}
Heat energy input (J)	q	0.138
Efficiency of in-situ system (%)	η	0.00026
Efficiency of Carnot cycle operating between same temperature limits (%)	η_{carnot}	3.6

5. SUMMARY AND CONCLUSION

5.1 Summary

In this work, the performance variation of graphene oxide based TCSC with electrode thickness, proton concentration and relative humidity have been studied. It was found that capacitance increases with electrode thickness and relative humidity. The capacitance showed a decreasing trend with increase in proton concentration because of higher pseudo-capacitance component due to higher H_2SO_4 concentration resulting in faster electrochemical degradation at high scan rate. The water uptake of TCSC was found to be about 150% at high RH of 82 % owing to strong hygroscopic nature of SGO. The electrical charge discharge behavior and capacitance retention of TCSC at different current densities were studied giving clarity on the range of current density that device needs to be operated for good performance and durability. The thermal charge-discharge behavior was studied in thermoelectric device setup and in situ under different heater surface temperatures. The voltage generated in the in-situ experiment was lower than that observed in thermoelectric measurement setup. This is because of underestimation of temperature difference by the IR camera which assumes perfectly black body for temperature estimation and also due to no heat sink unlike the thermoelectric measurement setup. The heat source when programmed to skin temperature of 34^0C gave a temperature of 6K across the TCSC and differential voltage of 10.02 mV. The efficiency analysis of TCSC was done assuming only radiation heat input from heat source to TCSC. The bimetal is mainly used for maintaining a steady temperature difference over time and also the mechanism is useful for continuously ON heat source applications and for intermittent ON and OFF heat source applications. The efficiency of the In-situ TCSC system was

computed to be 0.00026% compared to efficiency of Carnot cycle operating between the same temperature limits which is 3.6 %. However, efficiency computed here is the theoretical maximum efficiency as it was done with assumptions stated above but in reality, the efficiency is much lower. This analysis gives clarity on where the TCSC technology stands in comparison to other commercially available technologies like thermoelectric devices.

5.2 Conclusion

Thick modules of graphene oxide based thermally chargeable supercapacitor were prepared and better current and charge storage characteristics were observed. The charge storage and current improved with increase in humidity (RH% levels). The voltage generation of TCSC under different temperature gradients was measured with a thermoelectric measurement setup consisting of two peltier devices and the TCSC seebeck was estimated. The value of seebeck was found to be higher than the conventional thermoelectrics which is attributed to soret effect transport mechanism in TCSC. The in-situ thermal cycling setup was constructed to create a more realistic environment of device operation. A bimetal coil was used to cycle the TCSC and maintain the temperature gradient across the TCSC following which the voltage generation under conditions modeling body heat as energy source was calculated. The heat source when programmed to normal skin temperature resulted in a temperature difference of 6K across the TCSC and an output voltage of 10.02 mV. This work thus provides clarity on how thermally chargeable supercapacitors fare under realistic skin temperature operation conditions and gives us a good first-hand estimation of whether these devices can be practically applied to wearable and IOT electronics technology. This idea can be

further extended to any supercapacitor working on temperature gradient with modification in design and construction of in-situ setup depending on the supercapacitor geometry.

5.3 Future Work

The current work here has in-situ thermal cycling with intermittent heat source ON and OFF cycles. Thermal charging and discharging cycles with heat source switched ON continuously has more broader applications but it is a challenge to have cyclic motion when heat source is always at steady temperature. Two-way shape memory polymers can also be used for mounting the TCSC instead of bimetal. The shape memory polymers provide better sensitivity to temperature change and their deflection can be programmed unlike the bimetal. However, the strain retention rate of shape memory polymers tends to drop after few cycles which poses a challenge. Hence, the idea of thermal cycling if developed further can be incorporated into wearable devices which in turn can lead to potentially energy efficient wearable devices.

REFERENCES

1. Yu, C., et al., *Air-stable fabric thermoelectric modules made of N- and P-type carbon nanotubes.* Energy & Environmental Science, 2012. **5**(11): p. 9481-9486.

2. Kim, S.L., et al., *Flexible Power Fabrics Made of Carbon Nanotubes for Harvesting Thermoelectricity.* ACS Nano, 2014. **8**(3): p. 2377-2386.

3. Yu, C., et al., *Thermoelectric Behavior of Segregated-Network Polymer Nanocomposites.* Nano Letters, 2008. **8**(12): p. 4428-4432.

4. Kim, D., et al., *Improved Thermoelectric Behavior of Nanotube-Filled Polymer Composites with Poly(3,4-ethylenedioxythiophene) Poly(styrenesulfonate).* ACS Nano, 2010. **4**(1): p. 513-523.

5. Yu, C., et al., *Light-Weight Flexible Carbon Nanotube Based Organic Composites with Large Thermoelectric Power Factors.* ACS Nano, 2011. **5**(10): p. 7885-7892.

6. Wang, H., et al., *Simultaneously Improving Electrical Conductivity and Thermopower of Polyaniline Composites by Utilizing Carbon Nanotubes as High Mobility Conduits.* ACS Applied Materials & Interfaces, 2015. **7**(18): p. 9589-9597.

7. Hsu, J.-H., et al., *Origin of unusual thermoelectric transport behaviors in carbon nanotube filled polymer composites after solvent/acid treatments.* Organic Electronics, 2017. **45**: p. 182-189.

8. Kim, S.L., H.T. Lin, and C. Yu, *Thermally Chargeable Solid-State Supercapacitor*. Advanced Energy Materials, 2016. **6**(18): p. 1600546.

9. Kim, S.L., J.-H. Hsu, and C. Yu, *Intercalated graphene oxide for flexible and practically large thermoelectric voltage generation and simultaneous energy storage.* Nano Energy, 2018. **48**: p. 582-589.

10. Simon, P. and Y. Gogotsi, *Materials for electrochemical capacitors.* Nature Materials, 2008. **7**: p. 845.

11. Meng, C., et al., *Highly Flexible and All-Solid-State Paperlike Polymer Supercapacitors.* Nano Letters, 2010. **10**(10): p. 4025-4031.

12. Yuan, L., et al., *Paper-Based Supercapacitors for Self-Powered Nanosystems.* Angewandte Chemie International Edition, 2012. **51**(20): p. 4934-4938.

13. Anothumakkool, B., et al., *Novel scalable synthesis of highly conducting and robust PEDOT paper for a high performance flexible solid supercapacitor.* Energy & Environmental Science, 2015. **8**(4): p. 1339-1347.
14. Ramadoss, A., et al., *Piezoelectric-Driven Self-Charging Supercapacitor Power Cell.* ACS Nano, 2015. **9**(4): p. 4337-4345.

15. Wang, L., et al., *Flexible Solid-State Supercapacitor Based on a Metal–Organic Framework Interwoven by Electrochemically-Deposited PANI.* Journal of the American Chemical Society, 2015. **137**(15): p. 4920-4923.

16. Bae, S., et al., *Roll-to-roll production of 30-inch graphene films for transparent electrodes.* Nature Nanotechnology, 2010. **5**: p. 574.

17. Miller, J.R., R.A. Outlaw, and B.C. Holloway, *Graphene Double-Layer Capacitor with ac Line-Filtering Performance.* Science, 2010. **329**(5999): p. 1637.

18. Zhu, Y., et al., *Graphene and Graphene Oxide: Synthesis, Properties, and Applications.* Advanced Materials, 2010. **22**(35): p. 3906-3924.

19. El-Kady, M.F., et al., *Laser Scribing of High-Performance and Flexible Graphene-Based Electrochemical Capacitors.* Science, 2012. **335**(6074): p. 1326.

20. Gao, W., et al., *Direct laser writing of micro-supercapacitors on hydrated graphite oxide films.* Nature Nanotechnology, 2011. **6**: p. 496.

21. Chee, W.K., et al., *Flexible Graphene-Based Supercapacitors: A Review.* The Journal of Physical Chemistry C, 2016. **120**(8): p. 4153-4172.

22. Ghoniem, E., S. Mori, and A. Abdel-Moniem, *Low-cost flexible supercapacitors based on laser reduced graphene oxide supported on polyethylene terephthalate substrate.* Journal of Power Sources, 2016. **324**: p. 272-281.

23. Tyrrell, H.J.V. and R. Colledge, *Thermal Diffusion Potentials and the Soret Effect.* Nature, 1954. **173**: p. 264.

24. Platten, J.K., *The Soret Effect: A Review of Recent Experimental Results.* Journal of Applied Mechanics, 2005. **73**(1): p. 5-15.

25. Bonetti, M., et al., *Huge Seebeck coefficients in nonaqueous electrolytes.* The Journal of chemical physics, 2011. **134**(11): p. 114513.

26. Zhao, D., et al., *Ionic thermoelectric supercapacitors.* Energy & Environmental Science, 2016. **9**(4): p. 1450-1457.

27. Kim, B.C., et al., *Recent progress in flexible electrochemical capacitors: electrode materials, device configuration, and functions.* Advanced Energy Materials, 2015. **5**(22): p. 1500959.

28. Bahk, J.-H., et al., *Flexible thermoelectric materials and device optimization for wearable energy harvesting.* Journal of Materials Chemistry C, 2015. **3**(40): p. 10362-10374.

29. Ogata, C., et al., *All-graphene oxide flexible solid-state supercapacitors with enhanced electrochemical performance.* ACS applied materials & interfaces, 2017. **9**(31): p. 26151-26160.

30. Kim, B., et al., *Robust High Thermoelectric Harvesting Under a Self-Humidifying Bilayer of Metal Organic Framework and Hydrogel Layer.* Advanced Functional Materials, 2019. **29**(7): p. 1807549.